Engineering Structures 290 (2023) 116375

Contents lists available at ScienceDirect

Engineering Structures

journal homepage: www.elsevier.com/locate/engstruct

Seismic performance evaluation of novel RC frame structure with kinked rebar beams and post-yield hardening columns through shaking table tests

Shuijing Xiao [a], Guanzheng Zhou [a,b], Peng Feng [a,*], Zhe Qu [c]

[a] Department of Civil Engineering, Tsinghua University, Beijing, China
[b] Department of Civil Engineering, Faculty of Engineering, University of Hong Kong, Hong Kong, China
[c] Key Laboratory of Earthquake Engineering and Engineering Vibration, Institute of Engineering Mechanics, China Earthquake Administration, Yanjiao, Sanhe, Hebei, China

ARTICLE INFO

Keywords:
Novel RC frame structure
Kinked rebar
Post-yield hardening
Seismic performance
Strong column-weak beam
Self-centering capability

ABSTRACT

The kinked rebar configuration proposed by the authors has previously demonstrated improved seismic performance and progressive collapse resistance through quasi-static tests on reinforced concrete (RC) beams and plane RC frame substructures. In this paper, shaking table tests were conducted to evaluate the seismic performance of the novel RC frame structure with kinked rebar beams and post-yield hardening columns. The beams of the proposed frame included longitudinal bars with a kinked rebar configuration, while carbon fiber reinforced polymer (CFRP) bars were adopted in the columns to achieve post-yield hardening behavior. A 1/4-scale 4-story novel RC frame was designed, constructed, and tested, with three ground motion records of varying intensity levels used in the shaking table tests. The results showed that the inter-story and residual drift ratios of the proposed novel frame were effectively reduced compared to the conventional frame, indicating better seismic performance and self-centering capability. Additionally, the damage of the novel frame was first observed at beam ends and gradually became more severe with increasing seismic intensity. However, no obvious damage was observed at column ends, even under an extremely large earthquake. Thus, a “strong column-weak beam” failure mode of the novel RC frame structure was successfully achieved, and its repairability was effectively improved.

1. Introduction

The reinforced concrete (RC) frame, which comprises columns and beams, is widely used as a structural system worldwide. In conventional seismic design, the plastic hinges of the RC frame are expected to occur first on the beams, followed by the columns during earthquakes, resulting in a “strong column-weak beam” failure mode [1–4]. Unfortunately, previous investigations into structural damage during earthquakes [5–8] have shown that some RC frame structures designed according to existing seismic specifications have suffered more severe damage at column ends and beam-column joints, while the beams remained intact in certain conditions. This resulted in the failure of a “strong beam-weak column” mode, indicating that the seismic performance of conventional RC frames is inadequate.

To improve the seismic performance of RC frames, researchers have developed and studied various types of columns, beams, and beam-column joints [9–12]. Two main methods are employed to achieve the desired “strong column-weak beam” failure mode in RC frame structures: increasing the strength ratio of the column to the beam, and relocating the plastic hinges. However, determining the value of the strength ratio can be difficult, and the first method is usually not cost-effective. Therefore, the second method of developing novel configurations to relocate the plastic hinges of the RC frame has been widely studied [13–17]. Researchers, such as Hwang et al. [18], Park et al. [19], and Fenwick and Irvine [20] have proposed adding 45° bend-up bars, 90° bend-up bars, and reinforcement connecting plates, respectively, to strengthen the RC beam-column joint zone. Cyclic loading test results have shown that these novel joints improve energy dissipation and deformation, and reduce damage. Eom et al. [21], Teng et al [22], and Oudah and El-Hacha [23] proposed to reduce the size of beam end section, set horizontal rectangular opening at beam end, and set vertical joint at beam end respectively to achieve “strong column-weak beam” failure mode; results showed that these RC beam-column joints were well protected and their rotation capability were improved. Researchers

* Corresponding author.
E-mail address: fengpeng@tsinghua.edu.cn (P. Feng).

https://doi.org/10.1016/j.engstruct.2023.116375
Received 30 November 2022; Received in revised form 18 May 2023; Accepted 23 May 2023
Available online 31 May 2023

have also proposed replacing the concrete or longitudinal bars of the beam ends [24–26]. In recent years, self-centering RC beam-column joints, in which unbonded tendons were used to apply restoring force, have been developed and widely investigated to reduce residual displacement [27–29]. It should be noted that the above novel beam-column joint configurations of the RC frame are primarily developed to improve the lateral seismic behavior of the structure under an earthquake, and not necessarily consider its progressive collapse resistance.

The authors proposed a novel kinked rebar configuration (Fig. 1) to improve the seismic performance and progressive collapse resistance of RC frames [30–32]. As shown in Fig. 1(b), the conventional straight rebar is bent into a triangle or trapezoid shape to form the kinked rebar configuration. The kinked rebar has greater deformation capability while maintaining the same ultimate bearing capacity as the conventional straight rebar, as depicted in Fig. 1(c). The theoretical stress–-strain curve of the kinked rebar is divided into four stages by four key performance points, namely the first yield strainε_{y1}^{KB}, the first ultimate strainε_{u1}^{KB}, the second yield strainε_{y2}^{KB}, and the second ultimate strainε_{u2}^{KB}, respectively. Since the apparent first yield strength of the kinked rebar is lower than that of the straight steel rebar, the kinked rebar is placed at or near the inflection point (corresponding to the position where the bending moment of the beam in the normal state is zero) of the beams, as illustrated in Fig. 1(a) and (d). This allows the plastic hinge of the kinked rebar beam to effectively move to the inflection points, thereby the "strong beam-weak column" failure mode of RC frames can be achieved under seismic loads. Additionally, the kinked rebar can be straightened to assist the frame in resisting vertical loads, even at large deformations, and to prevent or delay collapse, as shown in Fig. 1(d). Previous studies have investigated the mechanical behavior of the kinked rebar under monotonic and cyclic loadings and provided a theoretical model (Fig. 1(c)) [30,32]. Furthermore, experimental investigations have been conducted on the monotonic and cyclic behavior of beams with kinked rebar configurations [30,32] and the progressive collapse behavior [31] of RC frame substructures with kinked rebar beams. These studies have demonstrated the effectiveness of the kinked rebar configuration in improving the seismic performance and progressive collapse resistance of the beam. However, the seismic performance of an entire RC frame structure with kinked rebar beams has not yet been studied.

The deformation capability of the RC frame is significantly affected by the bottom column, and the deformation of the conventional column may not match the deformation of the kinked rebar beam, resulting in unsatisfactory seismic performance and progressive collapse resistance of the structure. To address this issue, a post-yield hardening column is proposed in this study. Fig. 1(e) shows that the longitudinal reinforcements of the post-yield hardening column are replaced by carbon fiber reinforced polymer (CFRP) bars that exhibit linear behavior, allowing the column to exhibit positive post-yield stiffness (Fig. 1(f)). This modification enhances the proposed novel RC frame's deformation and self-centering capabilities. Additionally, the bottom column ends of the novel RC frame are strengthened by glass fiber reinforced polymer (GFRP) sheets to prevent severe column damage [33], as shown in Fig. 1(a). This paper evaluates the seismic performance of the proposed novel RC frame with kinked rebar beams and post-yield hardening columns through shaking table tests for the first time. The study begins by introducing the parameter design methods of the kinked rebar beam and the post-yield hardening column, followed by the construction of a 1/4-scale 4-story novel RC frame and a conventional contrastive RC frame. Shaking table tests were conducted on both structures, and their seismic responses and failure modes were compared. The shaking table test results confirm the satisfactory seismic performance of the proposed novel RC frame with kinked rebar beams and post-yield hardening columns.

2. Design and manufacture of the tested RC frame structure

2.1. Prototype RC frame structure

The prototype RC frame structure was designed in accordance with current Chinese codes [4,34], which are based on the elastic response spectrum and the internal forces are calculated using the minor earthquake. The building is intended to be situated in a high-risk seismic region, with a basic seismic acceleration of 0.2 g, and the site classification and design earthquake classification are assumed to be Type II

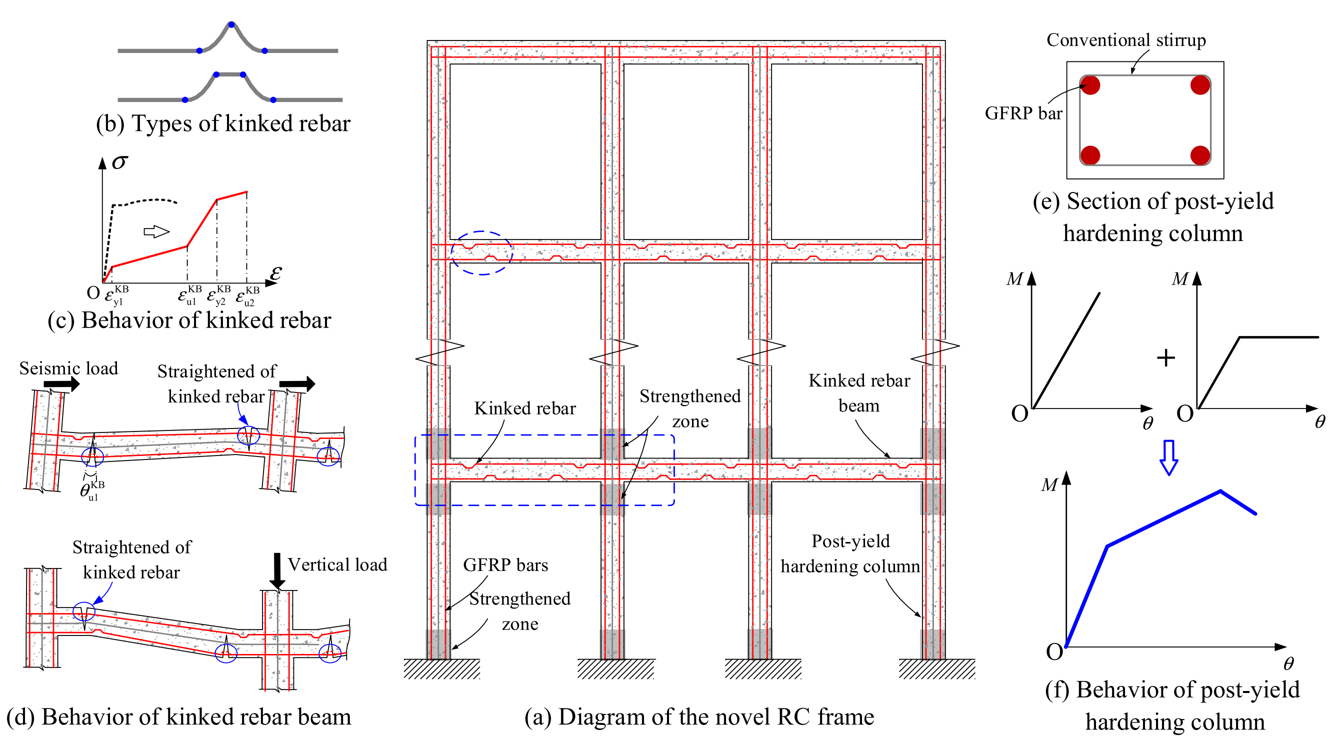

Fig. 1. Configuration of novel RC frame with kinked rebar beams and post-yield hardening columns.

and Group 2, respectively. The basic information of the prototype RC frame structure is depicted in Fig. 2. The 4-story building measures 36 m × 16 m in plan and 15.3 m in elevation, with five bays of equal length (7.2 m) in the x direction and two bays (10 m and 6 m, respectively) in the y direction. The first floor is 4.5 m high, while the rest of the floors are 3.6 m high, and the floor thickness is 0.12 m. The beam and column sizes, as well as the steel rebar information, are illustrated in Fig. 2. It should be noted that the section size and steel rebar of beams and columns in different floors are the same. As shown in Fig. 2(a), the designations “CC,” “SC,” “MC,” “BX,” and “BY” represent the corner column, side column, middle column, beam in x direction, and beam in y direction, respectively. The dead and live loads of the prototype structure are 6 kN/m^2 and 2.5 kN/m^2, respectively.

Since the prototype RC frame is symmetric in the x direction, the half-structure (between Axis 1 and Axis 3) was used for the model experiment, and the loads between Axis 3 and Axis 4 were added to the half-structure in proportion. Moreover, to meet the physical limitations of the available shaking table in the lab, a geometric scale factor of 1/4 was employed for the prototype half-structure. As a result, the plan dimensions, height of each story, and geometric sizes of beams, columns, and floor slabs of the test models were scaled to 1/4 those of the prototype RC frame. The scaling law and scale factors for the basic quantities are listed in Table 1. This study designed, tested, and compared a 1/4-scale 2 × 2 bay 4-story conventional RC frame structure and a 1/4-scale 2 × 2 bay 4-story novel RC frame structure.

2.2. Parameter design of the kinked rebar beam

The design parameters for the kinked rebar beam used in the novel frame are shown in Fig. 3. In this design, straight rebars are bent into a trapezoid shape at two symmetric positions along the one-bay beam, and the upper and lower kinked rebars are positioned at two sides of the beam’s inflection point, as demonstrated in Fig. 3(a). The size and dimensions of the kinked rebar beams in the novel frame are similar to those of the conventional frame and can be obtained using a dimension scale factor. For the novel beam with trapezoid kinked rebar, there are six main parameters (L_m, L_n, l_0, l_1, l_2, and l_3) that need to be determined, as illustrated in Fig. 3(a). Since the upper and lower kinked rebars are set near the inflection point, Eq. (1) can be used to calculate L_m and L_n.

$$L_m + 0.5L_n = \left(\frac{1}{2} - \sqrt{\frac{1}{4} - \frac{1}{3(2 + 1/K_B)}}\right)L \tag{1}$$

where L_m is the distance between the column edge and the center point of the upper kinked rebar, and L_n is the distance between the center points of the upper and lower kinked rebars. The span of the beam is denoted by L, and K_B represents the constraint stiffness of the beam end. Since the beam and column of the structure have a rigid connection, K_B can be considered to be infinitely large, simplifying Eq. (1) to $L_m + 0.5L_n = 0.211L$.

Due to the trapezoidal shape of the kinked rebar, which is embedded in the concrete, Eqs. (2)-(5) are proposed to determine the values of l_1, l_2, and l_3.

$$l_1 = \lambda(h - a_s - a_s') \tag{2}$$

$$l_2 = 0.5l_1 \tag{3}$$

$$L_n = 2l_1 + l_2 + l_3 \tag{4}$$

$$l_3 = l_1 \tag{5}$$

where l_1 and l_2 represent the horizontal axial projected length of the hypotenuse and the length of the upper base, respectively, of the trapezoid kinked rebar. The distance between the upper and lower kinked rebars is denoted by l_3. The values of a_s and a' s indicate the distance between the tension and compression longitudinal reinforcements and the beam edge, respectively, while h represents the height of the beam section. λ is a coefficient and its value is recommented to be taken from 0.25 to 0.35; in the structural design of this study, λ is taken as 0.25.

To ensure that the structure has sufficient collapse resistance, the kinked rebar is designed to be straightened when the inter-story drift ratio of the structure reaches 1/20, then Eq. (6) can be obtained.

$$\theta_{u1}^{KB} = \frac{L}{L - 2L_m - L_n} \times \frac{1}{20} \tag{6}$$

where θ_{u1}^{KB} is the rotation angle of the kinked rebar when straightened, as shown in Fig. 1(d), can be calculated using Eq. (7).

$$\theta_{u1}^{KB} = l_p^{KB}\varphi_{u1}^{KB} = l_p^{KB}\frac{\varepsilon_{u1}^{KB}}{h_0} \tag{7}$$

$$l_p^{KB} = l_2 + 2l_1 \tag{8}$$

$$\varepsilon_{u1}^{KB} = \frac{0.88(l_0 - l_1)}{(l_1 + 0.5l_2)} \tag{9}$$

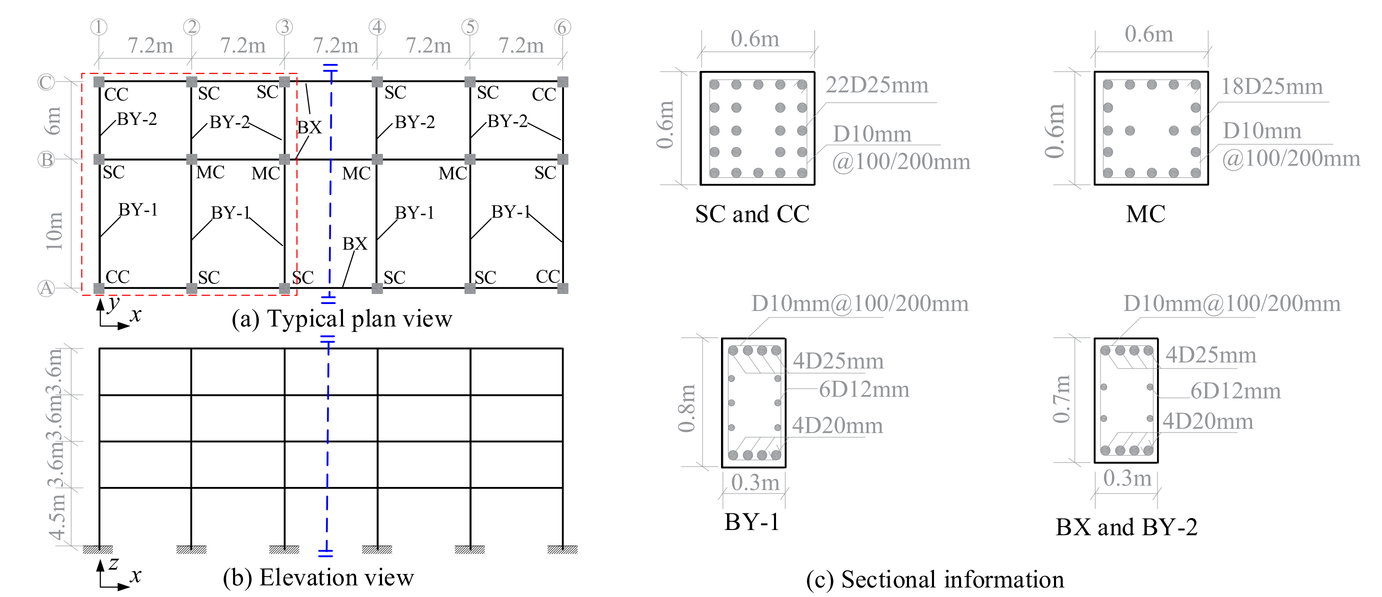

Fig. 2. The basic information of the prototype RC frame structure.

Table 1
Scale factors for the test model.

Basic quantity	Dimension	Elastic modulus	Equivalent density	Stress (strain)	Acceleration	Period (loading time)	Axial compression ratio
Scale lawing	S_L	S_E	S_ρ	$S_\sigma = S_\varepsilon$	S_a	$S_T = S_t$	S_u
Scale factor	1/4	1	1.199	1	3.33	0.27	1

Note: The materials of the scale model is the same with the prototype structure, thus $S_\sigma = S_\varepsilon = S_E = 1$; the added mass of the test model is limited by the shaking table, thus $1 < S_\rho < S_E/\ S_L$; $S_a = S_E/(S_L \cdot S_\rho)$;$S_t\ = S_L\sqrt{S_\rho/S_E}$

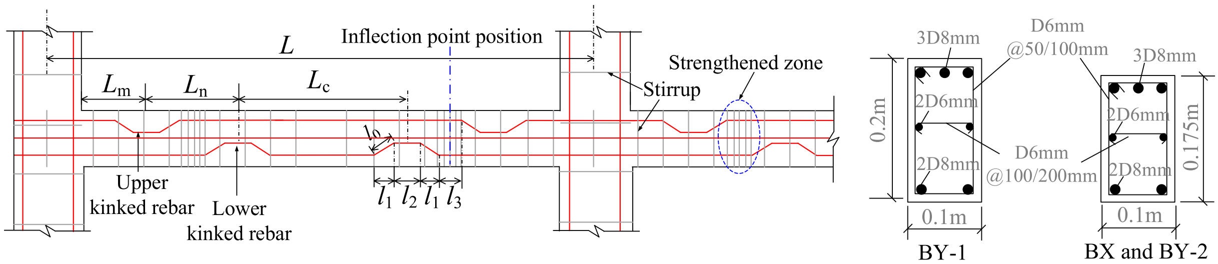

(a) Parameter of kinked rebar   (b) Parameter of beam section

Fig. 3. The design parameter of the kinked rebar beam for the novel frame.

where l_p^{KB} and φ_{u1}^{KB} are the length of the plastic hinge zone and the curvature of the kinked rebar, respectively; ε_{u1}^{KB} is the first ultimate strain of the kinked rebar, as shown in Fig. 1(c), and it corresponds to the strain of the kinked rebar when straightened and is evaluated using Eq. (9). Here, h_0 is the effective height of the beam and l_0 is the length of the hypotenuse of the trapezoid kinked rebar.

By using Eqs. (6)-(9), it is possible to derive Eq. (10) and consequently calculate l_0, thereby obtaining the six main parameters of the kinked rebar.

$$\frac{0.88(l_0 - l_1)(l_2 + 2l_1)}{(h - a_s - a_s^{'})(l_1 + 0.5l_2)} = \frac{L}{L - 2L_m - L_n} \times \frac{1}{20} \tag{10}$$

Based on the design parameters presented in Fig. 3 and the dimension scale factor, the values of the parameters for the kinked rebar beam in the novel frame are calculated and summarized in Table 2. The width b of the kinked rebar beam is adjusted to be 0.1 m to meet the requirement of the thickness of the concrete protective layer. The steel rebar details of the kinked rebar beams are shown in Fig. 3(b), and their reinforcement ratios are similar to those of the prototype beams. It is worth noting that the longitudinal reinforcements of the beams in the novel frame are designed to be kinked rebars and stirrups are added between the upper and lower kinked rebars to improve the shear capacity of the novel beam, as shown in Fig. 3(a). The kinked rebar is also used in the floor, and its parameters are the same as those in the novel beam. Other than that, the arrangement of the steel bars for the beams between the conventional and novel frames is the same.

2.3. Parameter design of the post-yield hardening column

The design information for the columns of both the conventional and novel frames is illustrated in Figs. 4 and 5, respectively. For the conventional column, the geometric dimensions and steel rebar are determined using the dimension scale factor S_L of 1/4. The cross-section of the column is 0.15 m × 0.15 m and four longitudinal reinforcements with a diameter of 12 mm are placed at the corner of SC, CC, and MC, while four longitudinal reinforcements with diameters of 10 mm and 8 mm are placed in the middle of SC and CC and MC, respectively, as shown in Fig. 4. A reserved hole with a diameter of 30 mm is also set at the center of the column for the application of prestress tendons, then the additional axial force can be applied through the prestress tendons during testing. In contrast, the novel frame's post-yield hardening column has the same cross-section size and corner reinforcements as the conventional column but replaces the middle longitudinal reinforcements with CFRP bars. As shown in Fig. 5, twelve longitudinal CFRP bars (three bars are combined at one same position) with a diameter of 6 mm are used at the middle of SC and CC, and eight longitudinal CFRP bars (two bars are combined at one same position) with a diameter of 6 mm are used at the middle of MC. The area of CFRP bars is designed to be similar to that of the corresponding conventional steel bars, and their elastic modulus (given in section 2.4) are also similar to that of the conventional steel bars. Therefore, the initial stiffness and yield capacity of the post-yield hardening column are considered to be similar to those of the conventional column in theory, with only the post-yield stiffness differing. Additionally, the bottom column ends of the post-yield columns at the first story of the novel frame are reinforced with GFRP sheets to protect the column from damage and improve their post-yield stiffness. Apart from these differences, the arrangement of the steel bars of columns between the conventional and novel frames is the same.

2.4. Model construction and material property

The construction of the model can be divided into two main steps: construction of the bottom foundation and construction of the upper

Table 2
Values of the designed parameters of the kinked rebar beam for the novel frame.

Number	b	h	a_s (a' s)	L	l_1 (l_3)	l_2	l_0	L_m	L_n
BX	0.1 m	0.175 m	20 mm	1.8 m	40 mm	20 mm	45 mm	310 mm	140 mm
BY-1	0.1 m	0.2 m		2.5 m				457.5 mm	
BY-2	0.1 m	0.175 m		1.5 m				246.5 mm	

Note: b is the width of the beam section.

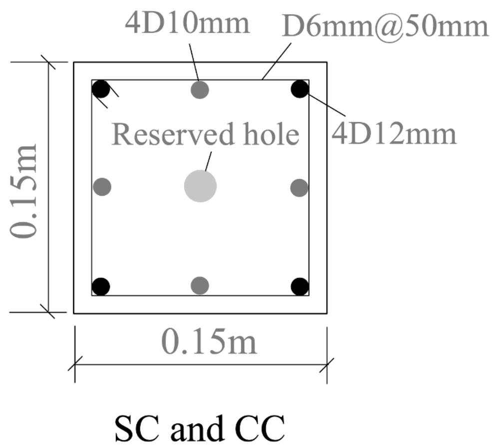

Fig. 4. Design information of columns of the conventional frame.

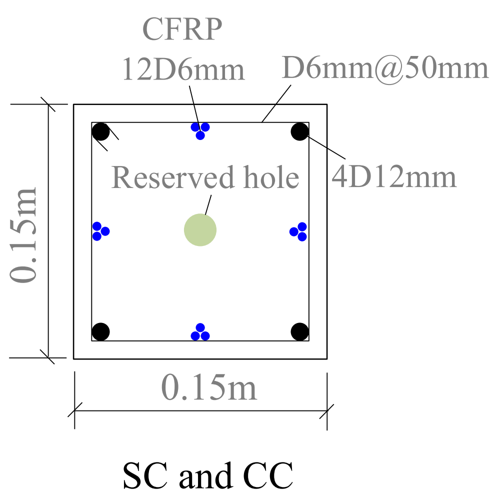

Fig. 5. Design information of post-yield hardening columns of the novel frame.

frame structure. The geometric size of the foundation is determined according to the base size of the shaking table, and reserved bolt holes are set. The reinforcement cage for the foundation is assembled, and the longitudinal bars of columns are positioned and placed in the cage (Fig. 6(a)). The foundation is then cast with concrete and cured (Fig. 6(b)). Next, the steel bars of the columns on the first story are assembled, and the wood templates of columns, beams, and floors are erected (Fig. 6(c)). The steel bars of beams and floors are then assembled correspondingly. The concrete for the columns, beams, and floors of the first story is cast and cured (Fig. 6(d)). The same process is repeated for the construction of the rest of the floors, with the completed three-dimensional models shown in Fig. 6(e) and (h). The construction processes for the conventional and novel frames are similar, with a few differences. For the novel frame, the wedge-type anchorage for CFRP bars of columns is embedded into the reinforcement cage of the foundation at the first step (Fig. 6(f)). The longitudinal reinforcement of beams and floors are bent to a trapezoid shape at corresponding positions before binding in the second step (Fig. 6(g)). Additionally, polyethylene foam is fixed on the kinked rebar to prevent bonding between steel bar and concrete, and the stirrups near the kinked rebar are strengthened (Fig. 6(g)). Strain gauges are attached to key positions of the steel bars to monitor the damage of the structure. Two layers of GFRP sheets with a thickness of 0.169 mm are attached around column ends at the first story of the novel frame using epoxy resin (Fig. 6(h)). Finally, 65 mass blocks (each weighing 20 kg) are placed on each floor slab, resulting in an actual seismic mass (including payload mass blocks) of 6100 kg for each floor and 7600 kg for the foundation.

After constructing two test models, the properties of concrete, steel bars, CFRP bars, and GFRP sheets were tested prior to the shaking table test of the structure. Compressive strength of concrete was obtained through a series of compressive tests on concrete cubes, resulting in values of 53.0 MPa, 44.1 MPa, 48.3 MPa, 48.8 MPa, and 47.7 MPa for the foundation, first, second, third, and fourth floors of the conventional frame, respectively. For the novel frame, the values were 50.0 MPa, 44.7 MPa, 40.8 MPa, 39.8 MPa, and 40.3 MPa for the foundation, first, second, third, and fourth floors, respectively. Mechanical properties of steel bars and CFRP bars were obtained through a series of tensile tests, whereas those of GFRP sheets were provided by the producer. The yield strength of steel bar with diameters of 14 mm, 12 mm, 10 mm, 8 mm, and 6 mm was 481 MPa, 484 MPa, 446 MPa, 461 MPa, and 376 MPa, respectively, while the ultimate tensile strength was 652 MPa, 644 MPa, 722 MPa, 770 MPa, and 504 MPa, respectively. The CFRP bar's tensile strength was 2075.5 MPa, and that of the GFRP sheet was 2200 MPa. The elastic modulus of steel bar with diameters of 14 mm, 12 mm, 10 mm, 8 mm, and 6 mm, CFRP bar, and GFRP sheet were 180 GPa, 184 GPa, 186 MPa, 191 GPa, 217 GPa, 157 GPa, and 100 GPa, respectively.

3. Experimental program

3.1. Test setup

The 1/4 scaled RC frame structures underwent shaking table tests at the Huixian Earthquake Engineering Comprehensive Lab of Institute of Engineering Mechanics, CEA, in Beijing, China. The shaking table had an

Fig. 6. Construction process and details of the test models.

overall dimension of 5 m × 5 m, a maximum payload capacity of 320 kN, a maximum velocity of 1.5 m/s, a peak ground acceleration (PGA) of 2 g, and a displacement range of ± 0.5 m. Fig. 7 shows an overall view of the test model on the shaking table. The model was secured to the shaking table base using high-strength bolts. Following fixation, axial force was applied to the columns via the tendons, and the force value was measured by a force sensor, as shown in Fig. 7. Nine force sensors were positioned at the top of the columns of the structure.

3.2. Instrumentation

To evaluate and monitor the seismic responses of two test models, accelerometers and displacement transducers were placed at corresponding positions, as illustrated in Fig. 8. The models were equipped with fifteen displacement transducers to record the lateral displacement: three on each story and three on the foundation. The displacement transducers numbered DX and DY were used to measure the displacement response of the structure in x and y directions, respectively. To

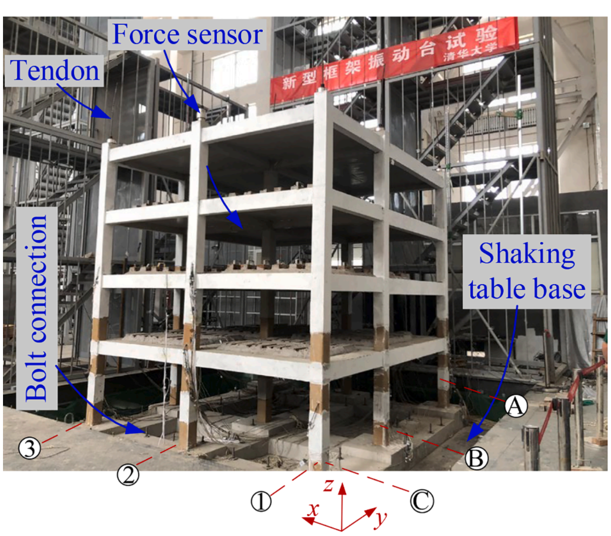

Fig. 7. Overall view of the test model on the shaking table.

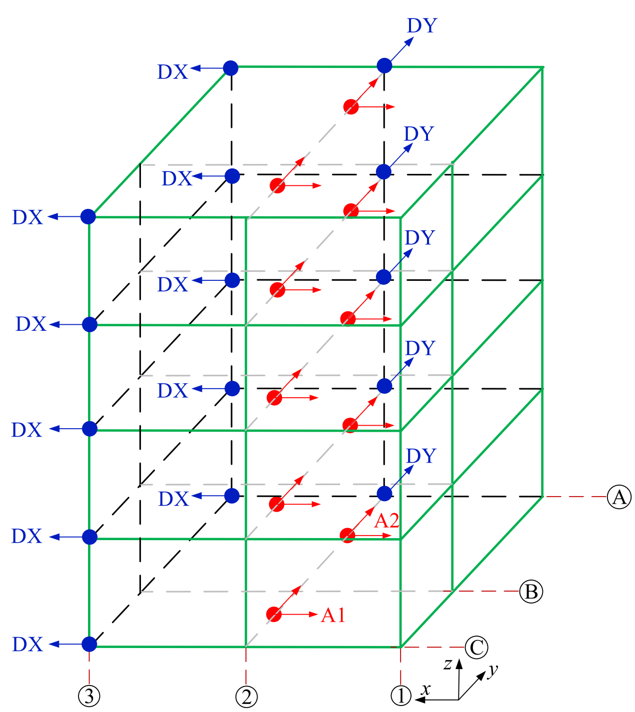

Fig. 8. Arrangement of accelerometers and displacement transducers.

account for the structure's asymmetry in the y direction, two displacement transducers were placed at different locations on the same floor, as shown in Fig. 8(a). The inter-story drift ratio of the model in the y direction was then calculated using the average values measured by the two displacement transducers at the same floor. The models also had eleven two-direction accelerometers mounted on them to record the acceleration during the test: two on each floor, two on the foundation, and one on the shaking table. The two-direction accelerations on the same floor were placed on the center of the middle beams between Axial C and Axial B (denoted as A1) and between Axial B and Axial A (denoted as A2), respectively, as shown in Fig. 8(a). The acceleration of the model was calculated by using the average values measured by the two accelerometers at the same floor.

3.3. Seismic inputs and test cases

Three main earthquake ground motion records were selected as the input excitations: the EL-Centro earthquake ground motion record, the Takatori earthquake ground motion record, and the Chichi earthquake ground motion record. The horizontal component with a larger peak ground acceleration (PGA) of each ground motion record was chosen. Fig. 9 displays the scaled acceleration time history and spectral acceleration of the selected ground motions. The ground motions were time-scaled by a factor S_t of 0.27 (Table 1).

Table 3 summarizes the test cases performed in this study. The seismic intensities of the EL-Centro and Takatori earthquake ground motions were considered based on the scale factor of acceleration (S_a = 3.33), and the PGAs were scaled to 0.24 g, 0.47 g, 0.67 g, 1.34 g, and 2.06 g. These two ground motions with their corresponding PGAs were separately applied in the x and y directions. Once the PGA reached 2.06 g, the EL-Centro and Takatori ground motions were simultaneously applied in both x and y directions. Additionally, the Chichi earthquake ground motion with a PGA of 2.06 g was applied to study the structural seismic collapse resistance and failure mode. The input PGAs in the x and y directions were kept the same during the bidirectional shaking table tests. To capture the changes in the natural frequencies of the test models, white-noise scanning was conducted after each test, as listed in Table 3.

Table 3
Test cases.

Cases	Input	PGA(g)		Cases	Input	PGA(g)	
		x	y			x	y
1	White-noise	0.12	–	25	White-noise	0.12	–
2	EL-Centro	0.24	–	26	EL-Centro	1.34	–
3	White-noise	–	0.12	27	White-noise	–	0.12
4	EL-Centro	–	0.24	28	EL-Centro	–	1.34
5	White-noise	0.12	–	29	White-noise	0.12	–
6	Takatori	0.24	–	30	Takatori	1.34	–
7	White-noise	–	0.12	31	White-noise	–	0.12
8	Takatori	–	0.24	32	Takatori	–	1.34
9	White-noise	0.12	–	33	White-noise	0.12	–
10	EL-Centro	0.47	–	34	EL-Centro	2.06	–
11	White-noise	–	0.12	35	White-noise	–	0.12
12	EL-Centro	–	0.47	36	EL-Centro	–	2.06
13	White-noise	0.12	–	37	White-noise	0.12	–
14	Takatori	0.47	–	38	Takatori	2.06	–
15	White-noise	–	0.12	39	White-noise	–	0.12
16	Takatori	–	0.47	40	Takatori	–	2.06
17	White-noise	0.12	–	41	White-noise	0.12	0.12
18	EL-Centro	0.67	–	42	EL-Centro	2.06	2.06
19	White-noise	–	0.12	43	White-noise	0.12	0.12
20	EL-Centro	–	0.67	44	Takatori	2.06	2.06
21	White-noise	0.12	–	45	White-noise	0.12	0.12
22	Takatori	0.67	–	46	Chichi	2.06	2.06
23	White-noise	–	0.12	47	White-noise	0.12	0.12
24	Takatori	–	0.67				

4. Results and discussions

4.1. Damage distribution and failure mode

During the shaking table tests, the crack development of both the conventional and novel frames was recorded and compared. The damage was primarily observed on the 1st and 2nd stories of both models, with the damage on the upper stories being minimal. Table 4 lists the main experimental observations for the structural members of both frames, and Fig. 10 compares the crack distribution of the conventional and novel frames under different seismic intensities in the y direction. When the peak ground acceleration (PGA) was 0.24 g, no significant cracks were observed on the conventional frame, while slight cracks occurred on the beam around the kinked rebar in the 1st and 2nd stories

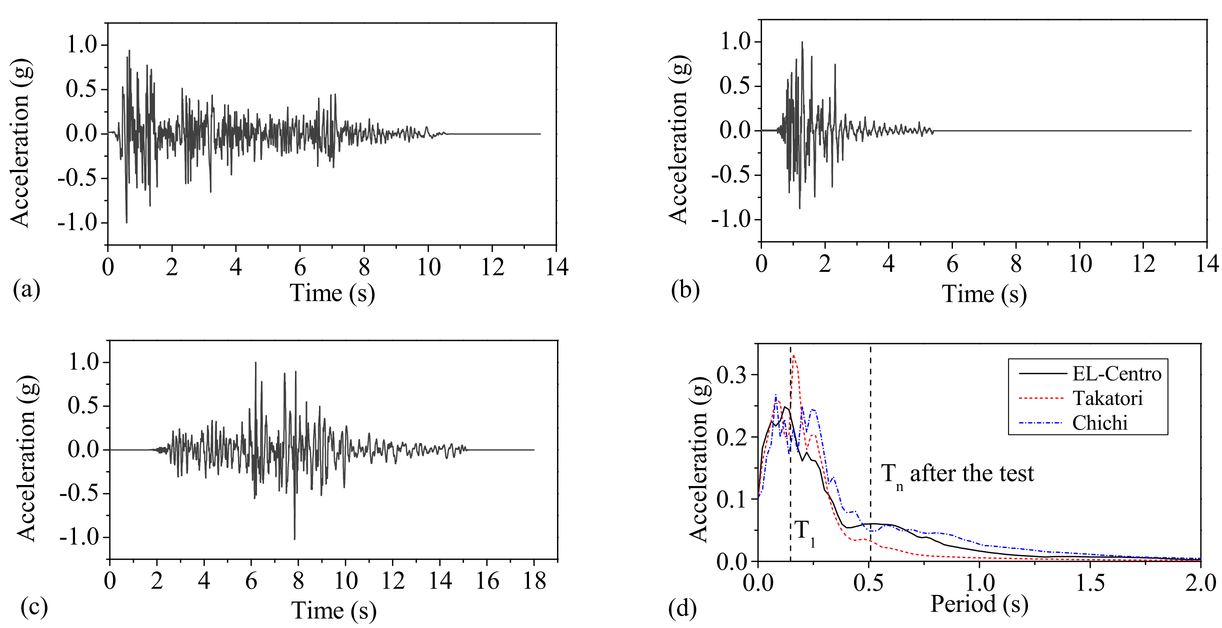

Fig. 9. Scaled acceleration time history and spectral acceleration of selected ground motions: (a) EL-Centro, (b) Takatori, (c) Chichi, and (d) comparisons of spectral accelerations.

Table 4
Experimental observations of the conventional and novel frames.

Cases	PGA	Description of the test observations	
		The conventional frame	The novel frame
2, 4, 6, 8	0.24 g	No obvious cracks.	Slight cracks occurred on beams in the 1st and 2nd stories (Fig. 10(a)).
10, 12, 14, 16	0.47 g	Minor cracks occurred on beams in the 1st story; slight lateral crack occurred on column ends in the 1st story.	More cracks developed on beams in the 1st and 2nd stories.
18, 20, 22, 24	0.67 g	Cracks extended on beams in the 1st story; Oblique crack occurred on beam-column joint in the 1st story; more slight lateral cracks on column ends in the 1st and 2nd stories.	Cracks developed and extended and crack width increased on beams in the 1st and 2nd stories.
26, 28, 30, 32	1.34 g	Cracks extended and more cracks developed on beams, columns and beam-column joints; crack width increased (Fig. 10(b)).	More slight cracks developed; two oblique cracks on the beam-column joint in the 1st story (Fig. 10 (b)).
34, 36, 38, 40	2.06 g	Cracks quickly developed on beam-column joint; concrete cover spalling on beam-column joint.	Cracks observed on all the beams in the 1st and 2nd stories; slight lateral cracks occurred on column ends in the 1st story.
42	2.06 g	Cracks extended and their width increased; concrete cover spalling on column ends in the 1st story.	Cracks extended and width increased on beams and column ends.
44	2.06 g	Concrete crushed on column ends and beam-column joints.	Several upper and lower cracks connected on beams; concrete cover spalling on one beam-column joint.
46	2.06 g	Severe damage on column ends and beam-column joints (Fig. 10(c)).	Concrete cover spalling on the beam in the 1st story (Fig. 10(b)).

of the novel frame, as shown in Fig. 10(a). However, both models remained elastic, meeting the design requirements under minor earthquakes. When the PGA was 0.47 g, minor cracks occurred on the beams, and slight lateral cracks occurred on column ends in the 1st story of the conventional frame. For the novel frame, more cracks developed only on the beams in the 1st and 2nd stories. Additionally, an oblique crack occurred on the beam-column joint in the 1st story, and more cracks were observed on columns in the 1st and 2nd stories of the conventional frame when the PGA reached 0.67 g. However, slender cracks were only observed on the beams of the novel frame, and the maximum width of the existing cracks was 0.3 mm when the PGA reached 0.67 g, which is helpful to straighten the kinked rebar. With the increase of PGA, cracks on beams, columns, and beam-column joints correspondingly increased. As shown in Fig. 10(b), two slight oblique cracks first occurred on the beam-column joint in the 1st story of the novel frame when the PGA was 1.34 g, while the maximum width of cracks on the beams and columns of the conventional frame reached 0.15 mm and 0.18 mm, respectively, indicating that the damage of the column of the conventional frame was more severe than that of the novel frame. When the PGA was 2.06 g, cracks quickly developed on the beam-column joints, and concrete crushed on column ends of the conventional frame. The damage of the conventional frame was especially severe under the Chichi ground motion with PGA of 2.06 g applied simultaneously in the x and y directions, as shown in Fig. 10(c). Although the number and width of cracks on beams of the novel frame quickly increased when the PGA reached 2.06 g, their positions were away from the beam ends, as shown in Fig. 10(c). In addition, the development of cracks on beam-column joints was well-controlled, with the maximum crack width of 0.2 mm, and concrete cover spalling was observed only on one beam-column joint.

Although the conventional RC frame did not collapse during the test, it was challenging to repair due to its severe damage on columns and beam-column joints after a strong earthquake. On the other hand, the repairability of the novel RC frame was improved as its damage mainly focused on beams.

Fig. 11 shows the final failure modes of the conventional and novel frames subjected to Chichi ground motion with a PGA of 2.06 g (Case 46). It can be seen that the conventional frame suffered from significant concrete spalling and reinforcement exposure on its columns and beam-column joints, and its damage was primarily concentrated on column ends or beam-column joints. In contrast, the novel frame's beams first showed and severely developed cracks due to the use of kinked rebar, whereas its columns' cracks were effectively controlled because of the utilization of CFRP bar and GFRP sheet. These findings indicate that the novel RC frame structure's damage was significantly reduced, and the "strong column-weak beam" failure mode was successfully achieved.

4.2. Dynamic characteristics

To indirectly reflect the stiffness degradation and damage condition of the structures during the tests, the structural period variation was examined by conducting white-noise tests before and after each shaking table test. The first three vibration modes of the models were translation in the x direction, translation in the y direction, and torsion, respectively. The estimated period variations of the two models are presented in Fig. 12. As the intensity of seismic excitation increased, the periods of both models gradually became longer, indicating a progressive degradation of structural stiffness. This was due to the development of minor cracks on beams, columns, and beam-column joints, as well as concrete cover spalling on column ends and beam-column joints, as discussed in Section 4.1.

The natural periods of the conventional frame in the x and y directions were 0.143 s and 0.141 s, respectively, while those of the novel frame were slightly greater at 0.147 s and 0.145 s, respectively, as shown in Fig. 12. This was attributed to the use of kinked rebar, which had a lower yield strength. As demonstrated in Fig. 12, the periods of both the conventional and novel frames rapidly increased after major earthquakes with a PGA of 1.34 g, which was consistent with the damage described in Fig. 10. From the beginning of the test to the last scan of white-noise, the periods of the conventional and novel frames increased by 2.7 times (both in x and y direction) and 2.4 times (both in x and y direction), respectively. This indicated that both structures sustained severe damage under strong earthquakes, while the damage of the novel frame was less severe than that of the conventional frame. This result was also consistent with the failure process shown in Table 4 and Fig. 11, which revealed that the novel RC frame structure effectively reduced damage and achieved the "strong column-weak beam" failure mode.

4.3. General seismic responses

Acceleration response of the test models was measured using accelerometers placed at each floor, and the peak acceleration of different stories under EL-Centro and Takatori ground motions with different PGAs were recorded and summarized in Tables 5 and 6, respectively. Generally, the maximum peak acceleration was observed at the top of the structures, while the peak acceleration of the foundation was similar to the input PGA value, indicating the models were well-fixed on the shaking table. Additionally, the peak accelerations of the conventional and novel frames gradually increased with increasing PGA values. When the input PGA value reached 1.34 g (corresponding to strong earthquake of the eighth degree area), the peak accelerations of both the conventional and novel frames in x and y directions were larger than 2.0 g, indicating significant potential for damage to structural components (Fig. 10(b)). However, the peak acceleration was not always continuously increased with the height of the story of the structures, as the peak accelerations of the lower stories may be larger than that of the upper stories. For instance, the peak accelerations in the x direction of the 2nd

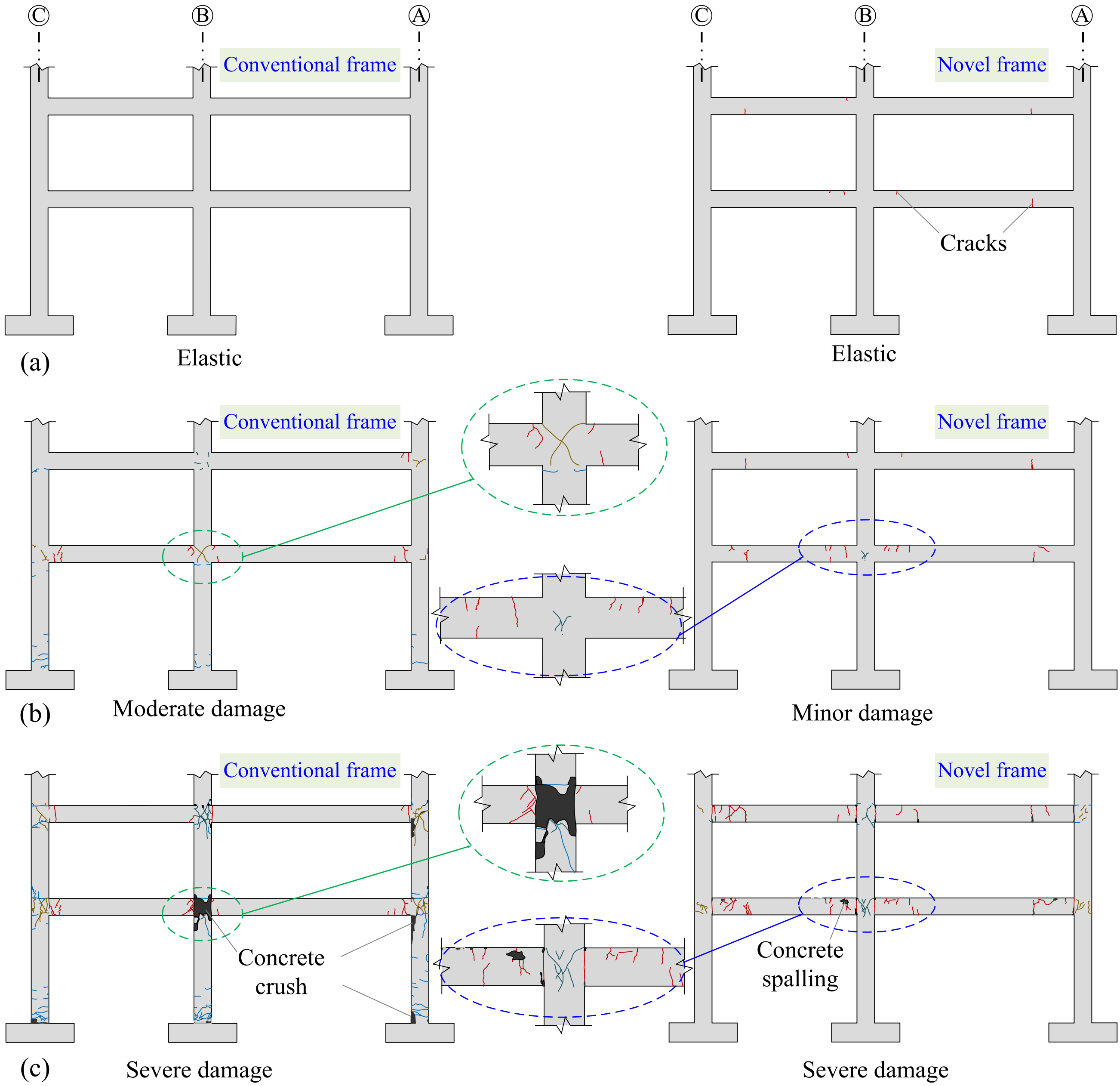

Fig. 10. Comparison of crack distribution of the conventional and novel frames under different seismic intensities in y direction: (a) PGA = 0.24 g (Case 8), (b) PGA = 1.34 g (Case 32), (c) PGA = 2.06 g (Case 46).

story of the conventional frame under EL-Centro ground motion with PGA of 0.24 g, 0.47 g, and 2.06 g were 0.59 g, 1.12 g, and 2.22 g, respectively, as listed in Table 5. These values were larger than that of the 3rd story, mainly due to the stiffness degradation of the structure. The variation of peak acceleration was more significant when the PGA reached 2.06 g, indicating that the damage accumulation of the test models was more severe under strong earthquakes.

The acceleration amplification factors, defined as the ratio of acceleration of each story to the acceleration of the foundation, in x and y directions of the two test models under EL-Centro ground motion with different PGAs are presented in Fig. 13. Generally, the acceleration amplification factors of the conventional and novel frames were similar. Additionally, it was observed that the acceleration amplification factors increased with the height of the story of both the conventional and novel frames. This variation was more regular in the y direction, as shown in Fig. 13(b). However, the acceleration amplification factor at each story of both the conventional and novel frames decreased as the PGA increased. This is because plastic hinges gradually formed at beam or column ends as the PGA increased, resulting in the structure attracting less seismic force and having greater damping. Therefore, the damage of both the conventional and novel frames gradually developed with the increase of PGA. The difference was that the damage of the conventional frame was mainly focused on columns and beam-column joints while the damage of the novel frame was mainly focused on beams.

The inter-story drift ratio distribution of the two test models under EL-Centro ground motion with different PGAs is shown in Fig. 14. The results indicated that the inter-story drift ratios in the x direction of each story of the conventional and novel frames increased with the increase of PGAs. The maximum inter-story drift ratio occurred at the first story for both structures, indicating that the most severe damage was concentrated at the first story. The variation of inter-story drift ratio in the y direction was similar to that in the x direction for both models. When the PGA was 0.24 g, the maximum inter-story drift ratios of the conventional and novel frames were less than 0.18 %, which meets the seismic design

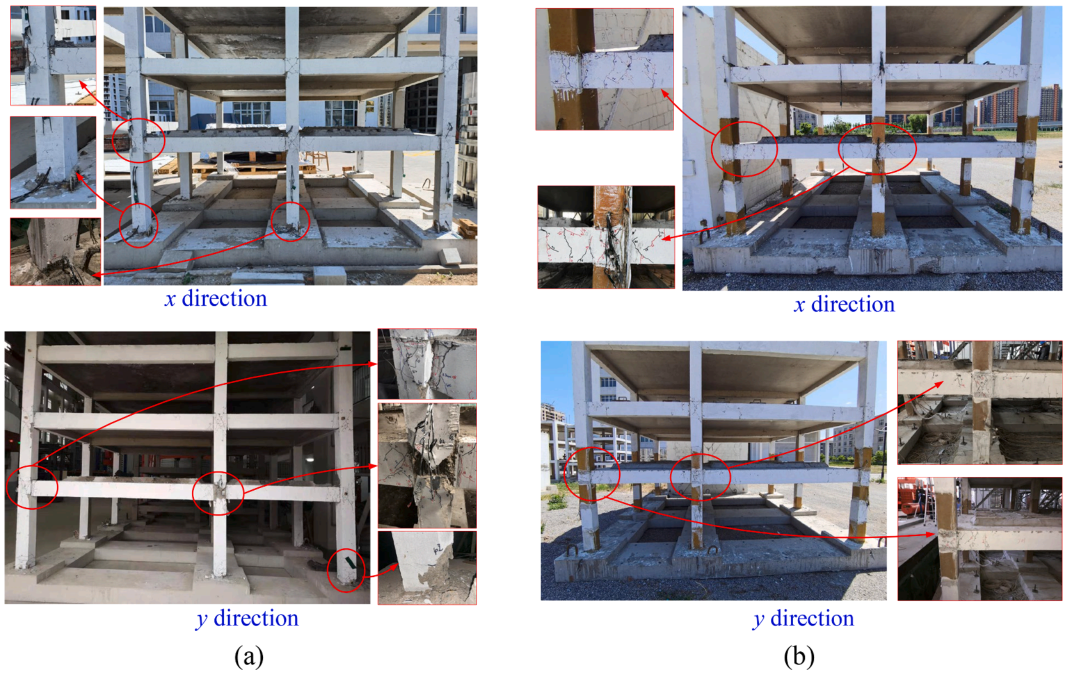

Fig. 11. Final failure modes: (a) Conventional frame, and (b) Novel frame.

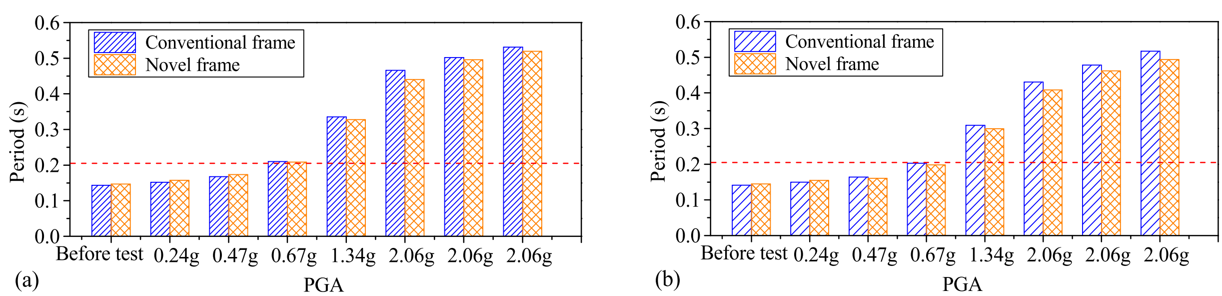

Fig. 12. Structural period variations after each test: (a) in x direction, and (b) in y direction.

Table 5
Peak acceleration of different stories under EL-Centro ground motion with different PGAs.

Models	Story	Peak acceleration in x direction (g)						Peak acceleration in y direction (g)					
		0.24	0.47	0.67	1.34	2.06	2.06-*xy*	0.24	0.47	0.67	1.34	2.06	2.06-*xy*
Conven-tional	4	0.68	1.12	1.41	2.07	2.64	2.72	0.82	1.35	1.27	2.40	3.14	2.43
	3	0.48	0.78	0.99	1.52	1.81	1.68	0.57	1.03	1.02	1.63	2.16	1.71
	2	0.59	1.12	0.98	1.52	2.22	1.79	0.51	0.89	1.07	1.69	2.25	2.13
	1	0.48	0.94	1.20	1.49	1.79	2.32	0.39	0.82	1.03	1.52	2.14	2.24
	0	0.32	0.58	0.74	1.30	2.01	1.88	0.21	0.44	0.67	1.34	1.79	2.03
Novel	4	0.59	0.93	1.23	2.12	3.04	2.83	0.65	1.12	1.27	2.28	2.95	2.58
	3	0.52	0.66	0.81	1.42	1.79	2.01	0.47	0.80	1.13	1.52	1.75	1.70
	2	0.54	0.80	0.76	1.39	2.31	2.15	0.46	0.75	1.10	1.46	2.06	2.00
	1	0.45	0.61	0.78	1.36	2.03	2.53	0.38	0.71	0.81	1.31	1.95	1.83
	0	0.30	0.41	0.63	1.29	2.06	2.06	0.20	0.42	0.65	1.30	1.95	2.05

Note: The notation 2.06-*xy* represents the seismic ground motion with PGA of 2.06 g that was applied simultaneously in both the x and y directions.

requirement for elastic inter-story drift ratio. As the PGA increased, the inter-story drift ratios of both models gradually increased, and the maximum inter-story drift ratios exceeded 1 % when the PGA reached 1.34 g (corresponding to a strong earthquake of the eighth-degree area), indicating that significant damage had occurred. Moreover, compared to the conventional frame, the inter-story drift ratios of the novel frame were lower when the PGA was less than 0.67 g and higher when the PGA was greater than or equal to 0.67 g. This is because the deformation of the kinked rebar in the novel frame was larger, and they gradually straightened when the PGA reached 0.67 g. However, the maximum inter-story drift ratios in both x and y directions of the novel frame were 6.5 % and 3.6 % lower, respectively, compared with the conventional frame when PGA was 2.06 g. This indicates that the novel frame had a better seismic performance than the conventional frame under strong earthquakes.

The reduction in maximum displacement and inter-story drift ratio was more significant when the structure entered the plastic stage during strong earthquakes. Figs. 15 and 16 compare the maximum

Table 6
Peak acceleration of different stories under Takatori ground motion with different PGAs.

Models	Story	Peak acceleration in *x* direction (g)						Peak acceleration in *y* direction (g)					
		0.24	0.47	0.67	1.34	2.06	2.06-*xy*	0.24	0.47	0.67	1.34	2.06	2.06-*xy*
Conven-tional	4	0.88	1.43	1.61	2.29	2.84	3.19	0.84	1.39	1.54	2.09	2.64	2.54
	3	0.55	1.02	1.30	1.71	1.91	1.66	0.63	0.86	1.29	1.68	1.97	1.32
	2	0.65	1.04	1.28	1.72	2.32	1.51	0.53	0.93	1.19	1.70	2.28	1.87
	1	0.53	0.74	0.91	1.39	1.69	2.02	0.39	0.69	0.87	1.35	1.89	2.51
	0	0.32	0.54	0.78	1.14	1.86	2.08	0.21	0.45	0.72	1.11	1.71	2.14
Novel	4	0.80	1.29	1.34	2.22	2.94	3.13	0.79	1.32	1.39	2.31	2.91	2.51
	3	0.61	0.82	1.01	1.61	1.69	1.65	0.64	0.96	1.03	1.67	1.89	1.62
	2	0.48	0.75	0.92	1.58	2.19	1.61	0.58	1.01	1.02	1.62	2.24	1.60
	1	0.41	0.57	0.76	1.33	2.03	2.16	0.36	0.77	0.81	1.36	1.96	1.67
	0	0.26	0.43	0.60	1.21	2.01	2.04	0.20	0.45	0.61	1.23	2.04	2.08

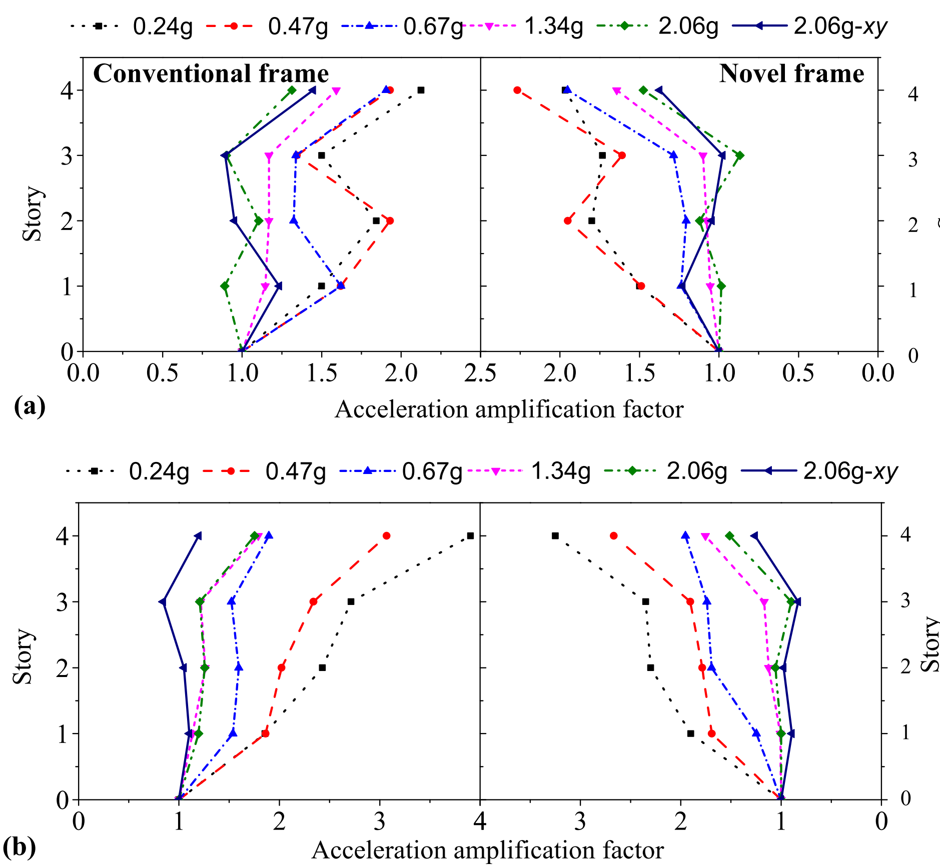

Fig. 13. Acceleration amplification factors of two test models under EL-Centro ground motion: (a) in *x* direction, and (b) in *y* direction.

displacement and inter-story drift ratio between the conventional and novel frames under different bidirectional strong earthquakes with a PGA of 2.06 g. The maximum displacement in both *x* and *y* directions of each story of the conventional and novel frames increased with the height of the structures, and the displacement increment of adjacent stories decreased with the increase of story height. This indicated that the deformation characteristic of both the conventional and novel frames was shear deformation, which is in accordance with the deformation of RC frame structures. The maximum displacement in *y* direction of the conventional and novel frames was greater than that in *x* direction due to the asymmetry of the two models in *y* direction. The maximum displacement of each story of the two structures under EL-Centro ground motion was larger than that under Takatori ground motion. The maximum displacement of each story of the two structures under Chichi ground motion was the largest among the three ground motions, resulting in the most severe damage under Chichi ground motion during the whole tests. Particularly, the maximum displacement in the *x* direction of the novel frame was relatively smaller than that of the conventional frame. The maximum displacement in *y* direction of the novel frame under EL-Centro and Takatori ground motions was similar to that of the conventional frame, while that of the novel frame under Chichi ground motion was relatively larger, mainly due to the more obvious asymmetry of the two frames in *y* direction after severe damaged.

The use of CFRP bars with elastic behavior in the novel frame resulted in a significant reduction of inter-story drift ratios in both *x* and *y* directions under different bidirectional strong earthquakes with PGA of 2.06 g, as shown in Fig. 16. In comparison to the conventional frame, the inter-story drift ratio distribution of the novel frame was more uniform under strong earthquakes. Specifically, the maximum inter-story drift ratios in *x* direction of the novel frame under EL-Centro, Takatori and Chichi ground motions were 1.56 %, 1.92 %, and 2.63 %, respectively, which were reduced by 20.3 %, 28.9 %, and 35.7 %, respectively, compared to the conventional frame. Correspondingly, the maximum

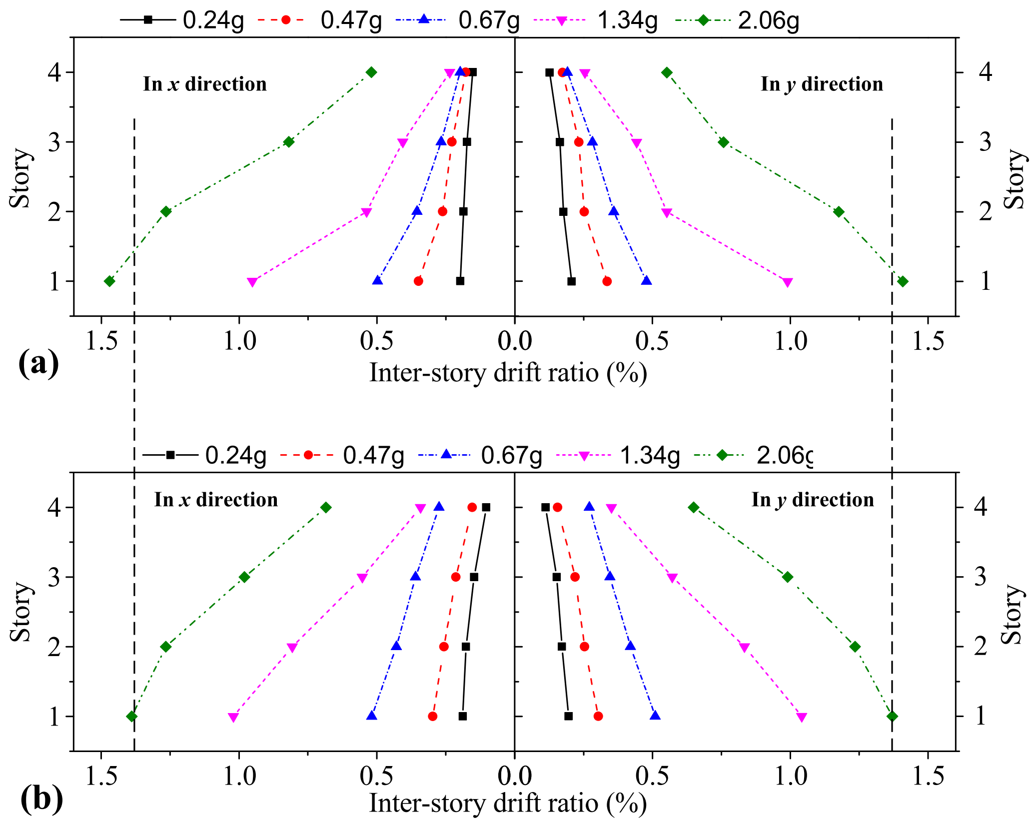

Fig. 14. Inter-story drift ratio distribution of two test models under EL-Centro ground motion: (a) the conventional frame, and (b) the novel frame.

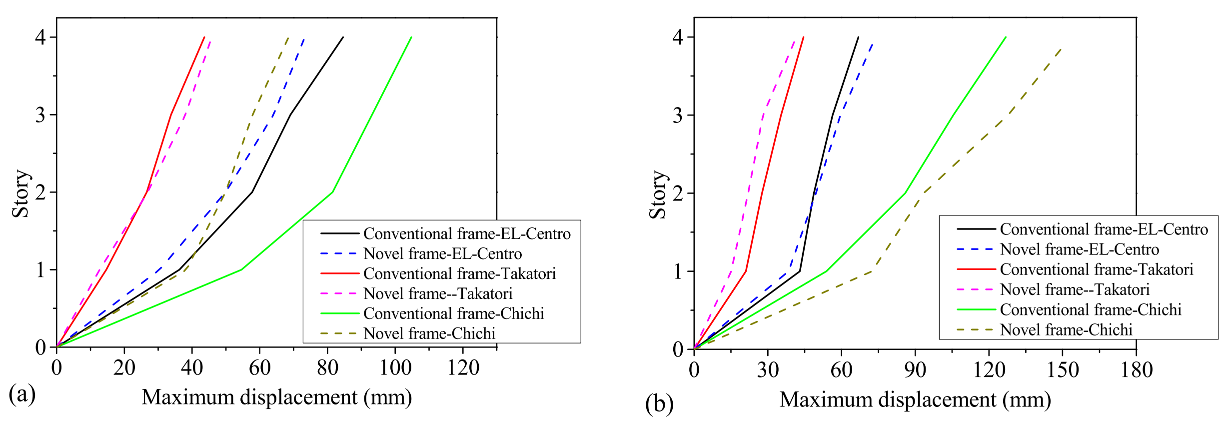

Fig. 15. Comparison of maximum displacement between the conventional and novel frames under different bidirectional strong earthquakes with PGA of 2.06 g: (a) in *x* direction, and (b) in *y* direction.

inter-story drift ratios in *y* direction of the novel frame under EL-Centro, Takatori and Chichi ground motions were reduced by 13.0 %, 22.5 %, and 27.8 %, respectively, compared to the conventional frame. Therefore, the seismic performance of the proposed novel RC frame structure was found to be satisfactory under strong earthquakes.

4.4. Residual displacement

Residual displacement is an essential parameter for evaluating the seismic resilience of a structure after an earthquake. The displacement of the conventional frame deviated from its original position during the test, thereby resulting in obvious residual displacement. In contrast, the novel frame returned to its original position with no obvious residual displacement after the earthquake. Fig. 17 compares the residual drift ratio, which is the ratio of residual displacement to the story height, between the conventional and novel frames under different bidirectional strong earthquakes with PGA of 2.06 g. The results indicate that the residual drift ratio in the bottom stories of the conventional frame was significantly greater than that in the upper stories, indicating severe damage focused mainly at the bottom. On the other hand, the residual drift ratio distribution of the novel frame was more uniform. Additionally, the residual drift ratio in each story of the novel frame under the same earthquake was smaller than that of the conventional frame, especially under Chichi ground motion, as shown in Fig. 17. For instance, when subjected to Chichi ground motion with PGA of 2.06 g, the maximum residual drift ratio in *x* and *y* directions of the conventional frame occurred in the first story, with values of 0.62 % and 0.97 %, respectively. These values were far greater than the repair limit value

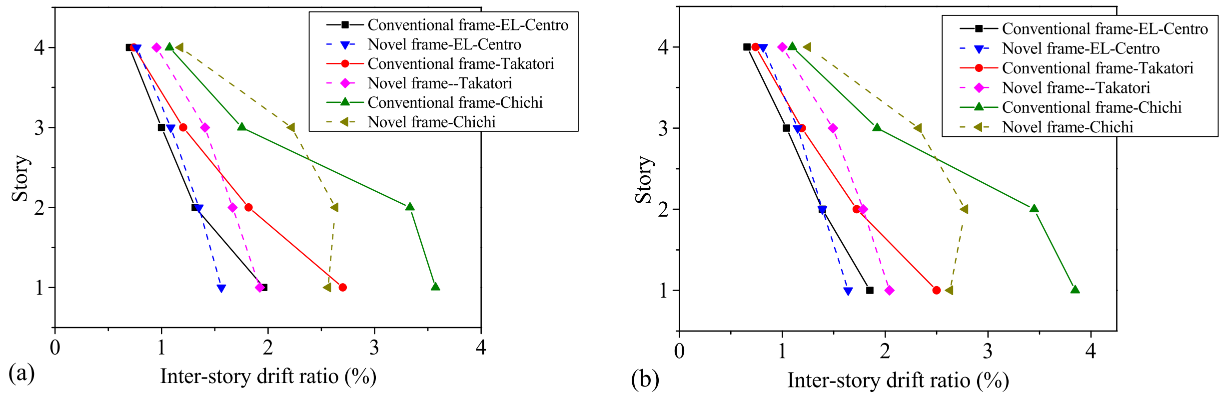

Fig. 16. Comparison of inter-story drift ratio between the conventional and novel frames under different bidirectional strong earthquakes with PGA of 2.06 g: (a) in *x* direction, and (b) in *y* direction.

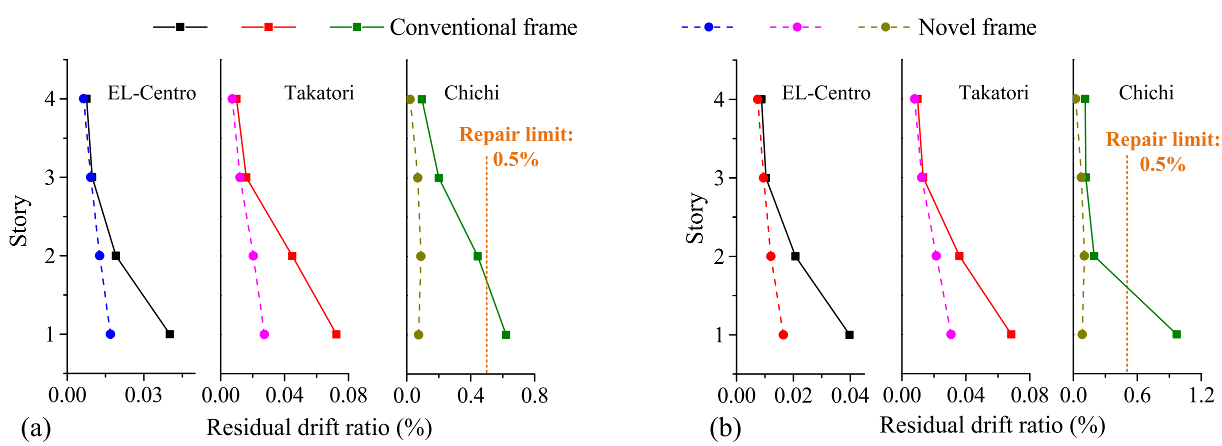

Fig. 17. Comparison of residual drift ratio between the conventional and novel frames under different bidirectional strong earthquakes with PGA of 2.06 g: (a) in *x* direction, and (b) in *y* direction.

of 0.5 %, indicating that the conventional RC frame was close to collapse and difficult to repair after subjecting to Chichi ground motion with PGA of 2.06 g. On the other hand, the maximum residual drift ratio in the *x* and *y* directions of the novel frame occurred in the second story with values of 0.07 % and 0.08 %, respectively, when subjected to Chichi ground motion. These values were 88.1 % and 89.2 % lower, respectively, than those of the conventional frame. Furthermore, the maximum residual drift ratios in the *x* and *y* directions of the novel frame were less than 0.5 %, indicating that the function of the novel frame could be restored through repair after subjecting Chichi ground motion with PGA of 2.06 g. Therefore, the seismic resilience of the proposed novel RC frame was significantly improved.

5. Conclusions

A novel RC frame included kinked rebar beam to realize “strong column-weak beam” failure mode and post-yield hardening column to improve seismic resilience was proposed in this paper. A 1/4-scale 4-story novel RC frame structure was designed and constructed. Then the seismic performance of this novel RC frame was investigated through a series of shaking table tests. The following conclusions can be drawn:

1. The results showed that the damage of the novel RC frame was effectively reduced compared to the conventional RC frame. Specifically, damage on the conventional RC frame gradually developed on column ends and beam-column joints with increasing seismic intensity, and it was severe when subjected to Chichi ground motion with PGA of 2.06 g (corresponding to the actual ground motion for a prototype structure was 0.62 g). In contrast, the damage on the novel frame was first observed on kinked rebar beams, and it became more severe with increasing seismic intensity due to the use of kinked rebars. However, the damage on columns was controlled due to the use of CFRP bars and GFRP sheets, thereby successfully achieving the desired “strong column-weak beam” failure mode.
2. The peak acceleration of the novel RC frame exhibited a similar pattern to that of the conventional RC frame, with the highest peak acceleration usually occurring at the top story and exceeding 2.0 g when the PGA reached 1.34 g. The peak acceleration amplification factors generally increased with the height of the story and decreased as the PGA increased, due to the accumulation of damage in the structure.
3. The inter-story drift ratio and residual drift ratio of the novel RC frame were effectively controlled when subjected to gradually increased PGAs, with more effective reduction observed when the structure entered the plastic stage under strong earthquakes. Compared to the conventional RC frame, the maximum inter-story drift ratios in the *x* and *y* directions of the novel RC frame under Chichi ground motion were reduced by 35.7 % and 27.8 %, respectively. The maximum residual drift ratio of the conventional RC frame under Chichi ground motion exceeded 0.5 %, while that of the novel RC frame was far less than 0.5 %, with the values of the maximum residual drift ratios in the *x* and *y* directions reduced by 88.1 % and 89.2 %, respectively. As a result, the seismic performance of the proposed novel RC frame structure was satisfactory under strong earthquakes, and its seismic resilience was effectively improved.

4. The construction process of the novel test model showed that the fabrication of the kinked rebar beam and the post-yield hardening column was straightforward and the construction of the novel structure was similar to that of conventional structures. This suggests that the proposed RC frame structure, with its satisfactory seismic performance, has a promising potential for practical engineering applications.

CRediT authorship contribution statement

Shuijing Xiao: Methodology, Investigation, Data curation, Writing – review & editing. **Guanzheng Zhou:** Methodology, Investigation, Data curation, Validation. **Peng Feng:** Conceptualization, Methodology, Supervision, Project administration, Funding acquisition, Writing – review & editing. **Zhe Qu:** Methodology, Validation.

Declaration of Competing Interest

The authors declare that they have no known competing financial interests or personal relationships that could have appeared to influence the work reported in this paper.

Data availability

Data will be made available on request.

Acknowledgements

The authors gratefully acknowledge the partial support of this research by the National Natural Science Foundation of China (No. 51778330), and the Institute of Guo Qiang, Tsinghua University (No. 2021GQI0007). This work has been supported by the New Cornerstone Science Foundation through the XPLORER PRIZE.

References

[1] ACI 318-14. Building code requirements for structural concrete. Farmington Hills: American Concrete Institute Michigan, 2014.
[2] Euro code 8. Design of Structures for Earthquake Resistance-Part1: General rules, seismic actions and rules for buildings. Bruxelles, 2004.
[3] Turkish Earthquake Code (TEC-2007). Regulations on structures constructed in disaster regions. Ministry of Public Works and Settlement, Ankara, 2007.
[4] GB50011-2010. Chinese Code for seismic design of buildings. Beijing, Ministry of Housing and Urban-Rural Development of the People's Republic of China, 2010.
[5] Sezen H, Whittaker AS, Elwood KJ, Mosalam KM. Performance of reinforced concrete buildings during the August 17, 1999 Kocaeli, Turkey earthquake, and seismic design and construction practise in Turkey. Eng Struct 2003;25(1):103–14.
[6] Rossetto T, Peiris N. Observations of damage due to the Kashmir earthquake of October 8, 2005 and study of current seismic provisions for buildings in Pakistan. Bull Earthq Eng 2009;7:681–899.
[7] Zhao B, Taucer F, Rossetto T. Field investigation on the performance of building structures during the 12 May 2008 Wenchuan earthquake in China. Eng Struct 2009;31:1707–23.
[8] Ahmadizadeh M, Shakib H. On the December 26, 2003, southeast Iran earthquake in Bam region. Eng Struct 2004;26:1055–70.
[9] Uma SR, Prasad AM. Seismic behaviour of beam-column joints in RC moment resisting frames: A review. Indian Concr J 2006;80(1):33–42.
[10] Xu LH, Zhang G, Xiao SJ, Li ZX. Development and experimental verification of damage controllable energy dissipation beam to column connection. Eng Struct 2019;199(4):109660.
[11] Yuksel E, Karadogan HF, Bal IE, Ilki A, Bal A, Inci P. Seismic behavior of two exterior beam–column connections made of normal-strength concrete developed for precast construction. Eng Struct 2015;99:157–72.
[12] Nie XF, Zhang SS, Teng JG, Chen GM. Experimental study on RC T-section beams with an FRP-strengthened web opening. Compos Struct 2018;185:273–85.
[13] Galunic B, Bertero VV, Popov EP. An approach for improving seismic behavior of reinforced concrete interior joints. Report UCB/EERC-70/30, Earthquake Engineering Research Center, Berkeley, CA; 1977. pp. 1–94.
[14] Ohkubo M, Hamamoto T. Developing reinforced concrete slotted beam structures to reduce earthquake damage and to enhance seismic structural performance. 13th World conference on Earthquake Engineering (13WCEE), 2004, 1-6 August, Vancouver, Canada.
[15] Muir CA, Bull DK, Pampanin S. Seismic testing of the slotted beam detail for reinforced concrete structures, ASCE-Structures Congress, 2013, 2-4 May, Pittsburgh, Pennsylvania, United States.
[16] Kam WY. Selective weakening and post-tensioning for the seismic retrofit of non-ductile RC frames. University of Canterbury; 2010 [PhD thesis].
[17] Kam WY, Pampanin S, Elwood K. Seismic performance of reinforced concrete buildings in the 22 February Christchurch (Lyttleton) Earthquake. Bull New Zealand Nat Soc Earthq Eng 2011;44(4):239–78.
[18] Hwang HJ, Eom TS, Park HG. Design considerations for interior RC beam–column joint with additional bars. Eng Struct 2015;98:1–13.
[19] Park R, Milburn JR. Comparison of recent New Zealand and United States seismic design provisions for reinforced concrete beam-column joints and test results for four units designed according to the New Zealand code. Bull N Z Soc Earthq Eng 1983;16(1):21–42.
[20] Fenwick RC, Irvine HM. Reinforced concrete beam column joints for seismic loading. Bull N Z Soc Earthq Eng 1977;10(3):121–8.
[21] Eom TS, Park HG, Hwang HJ, Kang AM. Plastic hinge relocation methods for emulative PC beam-column connections. J Struct Eng 2015;142(2):04015111.
[22] Teng JG, Zhang SS, Jing DH, Nie XF, Chen GM. Seismic retrofit of RC frames through beam-end weakening in conjunction with FRP strengthening. Proceeding in the 4th Asia Pacific Conference on FRP in Structures (APFIS), Melbourne, Victoria, Australia, 11-13 December; 2013.
[23] Oudah F, El-Hacha R. Plastic hinge relocation in concrete structures using the double-slotted-beam system. Bull Earthq Eng 2017;15(5):2173–99.
[24] Youssef MA, Nehdi MSAM. Experimental investigation on the seismic behavior of beam-column joints reinforced with superelastic shape memory alloys. J Earthq Eng 2008;12(7):1205–22.
[25] Wu YF, Zhou YW. Controlling the damage of concrete columns through compression yielding. Struct Control Health Monit 2011;18(8):890–907.
[26] Wu YF, Zhou YW, He XQ. Performance-based optimal design of compression-yielding FRP-reinforced concrete beams. Compos Struct 2010;93(1):113–23.
[27] Cai XN, Pan ZF, Zhu YZ, Gong NN, Wang YW. Experimental and numerical investigations of self-centering post-tensioned precast beam-to-column connections with steel top and seat angles. Eng Struct 2021;226:111397.
[28] Song LL, Guo T, Chen C. Experimental and numerical study of a self-centering prestressed concrete moment resisting frame connection with bolted web friction devices. Earthq Eng Struct Dyn 2014;43:529–45.
[29] Wang HS, Marino EM, Pan P. Design, testing and finite element analysis of an improved precast prestressed beam-to-column joint. Eng Struct 2019;199:109661.
[30] Qiang HL, Feng P, Stojadinovic B, Lin HW, Ye LP. Cyclic loading behaviors of novel RC beams with kinked rebar configuration. Eng Struct 2019;200:109689.
[31] Qiang HL, Yang JX, Feng P, Qin WH. Kinked rebar configurations for improving the progressive collapse behaviours of RC frames under middle column removal scenarios. Eng Struct 2020;211:110425.
[32] Feng P, Qiang HL, Qin WH, Gao M. A novel kinked rebar configuration for simultaneously improving the seismic performance and progressive collapse resistance of RC frame structures. Eng Struct 2017;147:752–67.
[33] Wang ZY, Li ZY, Yang JQ, Huang FS, Feng P. Axial compressive and seismic performance of GFRP wrapped square RC columns with different scales. J Build Eng 2022;62:105342.
[34] GB 50010-2010. Chinese Code for design of concrete structures. Beijing, Ministry of Housing and Urban-Rural Development of the People's Republic of China, 2010.